Simulation of Semiconductor Processes and Devices 2016
Edited by E. Bär, J. Lorenz, and P. Pichler

Metal-InGaAs contact resistance calculations from first principles

Troels Markussen and Kurt Stokbro
QuantumWise A/S
Fruebjergvej 3, Postbox 4
DK-2100 Copenhagen, Denmark
Email: troels.markussen@quantumwise.com

***Abstract*—The metal-semiconductor contact resistance is an important factor in the performance of MOSFETs and a detailed understanding of the contact resistance is necessary in order to simulate and eventually optimize the devices. In this work we calculate metal-InGaAs contact resistances using Density Functional Theory (DFT) combined with non-equilibrium Greens function (NEGF) methods as implemented in Atomistix ToolKit (ATK). We have calculated specific contact resistivities, ρ_c, of metal-InGaAs and metal-InAs interfaces, where the metals studied are Ti, W, and Mo. We find that ρ_c is approximately inversly proportional to the doping density with values that are in close agreement with experimental results from the literature.**

I. Introduction

Interfaces between metals and semiconductors occur in a wide range of technologies such as electronic and optoelectronic devices, thermoelectric modules, as well as quantum computing devices[1]. The metal-semiconductor contact resistance is an important factor in the performance of both MOSFETs[2] and thermoelectrics[3] and a detailed understanding of the contact resistance is necessary in order to simulate and eventually optimize the devices.

In this work we report on theoretically calculated contact resistances. The calculations are performed with Density Functional Theory (DFT) combined with non-equilibrium Green's function (NEGF) methods as implemented in ATK[4]. This approach allows for first-principles studies of arbitrary material combinations and does not require fitted parameters as is the case for e.g. tight-binding (TB) methods. The DFT-based approach is thus particularly well suited for interface studies as TB parameters between metals and semiconductors are generally not available in the literature.

We have calculated specific contact resistivities of metal-$In_{0.5}Ga_{0.5}As$ and metal-InAs interfaces, where the metals studied are Ti, W, and Mo, which have been studied experimentally [5]. We further study both In- and As terminated semiconductor surfaces. For both metal-InAs and metal-InGaAs interfaces the calculated specific contact resistivities are in close agreement with experimental values.

II. Method

A. Metal-InGaAs interface atomic structure

When studying an interface the first step is to setup an appropriate atomic configuration. In all calculations presented below, the $In_{0.5}Ga_{0.5}As$ is oriented such that the [001] direction is normal to the interface plane. We do not simulate $In_{0.5}Ga_{0.5}As$ as a random alloy, but always represent it with periodically repeated alternating planes of In-As-Ga-As-In-etc.

The orientation of the metal has been chosen as a compromise between minimizing the strain, which is always applied to the metal, and at the same time keeping the system size computationally feasible. The average strain applied to the metal is never larger than 5%. Since we are not aware of any experimental results for the crystal orientation of the metal, we have generally taken the liberty to choose a metal orientation that minimizes the strain with the smallest possible super-cell area.

Having defined an initial interface structure, we first form a slab geometry periodic in x and y but with finite sizes of Ti and InGaAs in the z-direction and with a large vacuum region. We then allow for a structural relaxation of the atoms closest to the interface. The remaining atoms are allowed to move as a rigid body, i.e. their internal coordinates are fixed and only the centre of mass is moved [6]. The structural relaxation is performed until the maximum force on all the freely moving atoms (close to the interface) is below 0.05 eV/Å. The structural relaxation is performed with the Perdew-Burke-Ernzerhof (PBE) [7] generalized gradient approximation for the exchange-correlation potential with a transverse k-point density of typically 6 Å (this corresponds to having one k-point in a direction with real space unit cell length of $2\pi \times 6$ Å). The right end of the $In_{0.5}Ga_{0.5}As$ which is facing vacuum is passivated using hydrogen atoms in order to avoid metallic surface states.

Having relaxed the interface, we construct a device configuration by extending both the metal and $In_{0.5}Ga_{0.5}As$ using the fixed structures at the ends. The device configuration consists of a central region shown in Figure 1 connected to two semi-infinite electrodes. The atomic structure as well as the potentials are fully periodic in the electrodes, whereas in the central region there can be a non-periodic potential profile as will be shown below.

B. Device calculations

For the device calculations we have used the Meta-GGA exchange-correlation functional by Tran and Blaha [8] with

978-1-5090-0818-6/16/$31.00 ©2016 IEEE

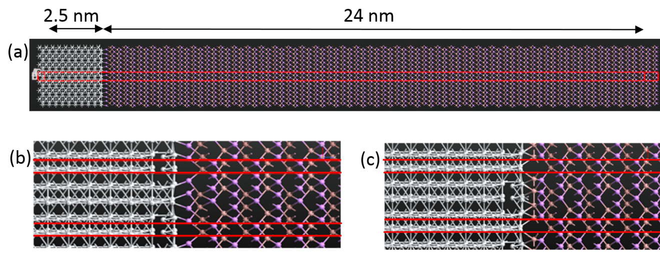

Fig. 1. Ti-InGaAs device structure (a). The central region consists of a relatively short Ti region and a long InGaAs region in order to properly describe the screening of the electrostatic potential. The central region contains 372 atoms. The detailed interface structures for an As terminated InGaAs is shown in (b) and for an In terminated InGaAs in (c). The red boxes indicate the calculation unit cell.

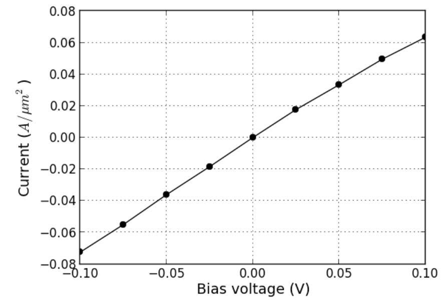

Fig. 2. IV curve for a Ti-$In_{0.5}Ga_{0.5}As$ interface. The $In_{0.5}Ga_{0.5}As$ has an As surface and a doping level of $n = 10^{19}\,\mathrm{cm}^{-3}$. The current is calculated from self-consistent finite-bias DFT-NEGF calculations. The linear IV curve shows that the contact is Ohmic with a resistance of 1.4 $\Omega\mu\mathrm{m}^2$.

a c-parameter fitted to yield the experimental band gap of $In_{0.53}Ga_{0.47}As$ (0.74 eV). The transverse k-point sampling used for the device calculations is three times higher than for the structural relaxation in order to get an accurate determination of the Fermi levels, which is important for the transport but much less important for the structural relaxation.

In the device calculations, the semiconductor region is n-doped. In ATK the doping is modeled with an effective scheme by introducing localized charges bound to the individual silicon atoms [9]. The localized charges, centered around the atoms, have the opposite sign of the desired doping density, which acts as a carrier attractor by modifying the electrostatic potential on the atom. For a bulk system, the compensation charge added to each atom is neutralized by explicitly adding a valence charge of the opposite sign, so that the system remains charge neutral. For a device structure, the compensation charge is neutralized implicitly by the carriers provided by the reservoirs, and the system is maintained charge neutral under the condition that the intrinsic electric field in the system is zero.

C. Calculating the contact resistance

It has been experimentally found that heavily doped device regions form Ohmic contacts with the metals [5]. A first step in our analysis is to verify this result by calculations. Figure 2 shows the IV curve of the Ti-InGaAs device given in Figure 1. At relatively low bias voltages the current increases linearly with voltage showing that the contact indeed forms an Ohmic resistance. The contact resistance could be estimated from the slope of the IV curve at zero applied bias giving a value of 1.4 $\Omega \mu m^2$. However, part of the resistance obtained from Figure 2 is due to the finite carrier density in the $In_{0.5}Ga_{0.5}As$ and in principle also in the metal, but the number of metal states at the Fermi energy is much larger than the $In_{0.5}Ga_{0.5}As$ states and the metal contribution to the resistance can safely be neglected. If instead we would simulate a pure $In_{0.5}Ga_{0.5}As$ device, where obviously the contact resistance is zero, we would still obtain a linear IV curve with a certain slope. Hence, it is clear that the IV curve cannot be used directly to obtain the contact resistance, although it might provide a reasonable estimate.

In order to obtain an expression for the contact resistance, which does not include the contribution from the finite InGaAs carrier density we take the following approach. From zero-bias calculations we calculate the transmission coefficient of the device, $T_{dev}(E)$, from which we obtain the zero-bias conductance as

$$G_{dev} = \frac{2e^2}{h} \int T_{dev}(E) \left(-\frac{\partial f}{\partial E} \right) \mathrm{d}E, \tag{1}$$

where f is the Fermi-Dirac distribution. Similarly we calculate the transmission coefficient of a pure InGaAs device, $T_{InGaAs}(E)$, and calculate a zero-bias conductance G_{InGaAs} as in Eq. (1). The corresponding resistances are simply $R_{dev} = 1/G_{dev}$ and $R_{InGaAs} = 1/G_{InGaAs}$. We now define the total device resistance as a sum of the intrinsic InGaAs resistance plus a contact resistance, R_c: where f is the Fermi-Dirac distribution. Similarly we calculate the transmission coefficient of a pure InGaAs device, $T_{InGaAs}(E)$, and calculate a zero-bias conductance G_{InGaAs} as in Eq. (1). The corresponding resistances are simply $R_{dev} = 1/G_{dev}$ and $R_{InGaAs} = 1/G_{InGaAs}$. We now define the total device resistance as a sum of the intrinsic InGaAs resistance plus a contact resistance, R_c:

$$R_{dev} = \frac{1}{G_{dev}} = R_c + R_{InGaAs} \tag{2}$$

Equation (2) thus defines the contact resistance R_c. The specific contact resistivity is then simply $\rho_c = R_c \cdot A$, where A is the cross sectional area of the calculation unit cell. We notice that in the case where the device would have been two pieces of InGaAs joint to form an infinite InGaAs system, $R_{dev} = R_{InGaAs}$ resulting in $R_{contact} = 0$ as it should. In doing so, for the Arsenic terminated surface the specific contact resistivity of the Ti-InGaAs interface comes out as 0.99 $\Omega \mu m^2$, i.e. slightly lower than the value obtained from the IV curve because the internal InGaAs resistance has been subtracted. The difference between R_c and R_{dev} is generally larger for low doping values.

Figure 3 (left) shows the transmission function of the pure InGaAs (black) together with Ti-InGaAs transmission where

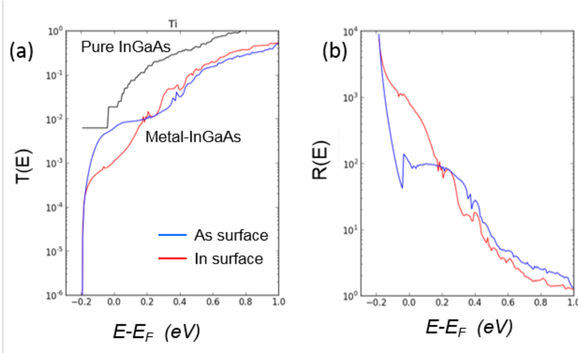

Fig. 3. Transmission (a) and energy-resolved contact resistance (b) for Ti-InGaAs interfaces. The blue curves corresponds to an interface where InGaAs is terminated by As (Fig. 1 (b)), while the red curves represent In termination (Fig. 1 (c))

TABLE I
CALCULATED AND EXPERIMENTAL SPECIFIC CONTACT RESISTIVITIES (IN UNITS OF $\Omega\mu m^2$) AT $n = 2 \cdot 10^{19}$CM^{-3}. IN THE CASE OF INGAAS, THE CALCULATED RESULTS SHOW VALUES FROM IN, AS TERMINATED SURFACES, WHILE FOR INAS, ONLY AS TERMINATED SURFACES WERE CONSIDERED. [a]: REF. [5], [b]: REF. [12]

	Calculations	Experiment
	InGaAs	
Ti	0.7, 4	4[a]
W	2, 10	46.5[a]
Mo	8, 7	7.9[a]
	InAs	
Ti	1.2	1.2 – 1.4[a]
Mo	1.8	1.2[b]

the blue and red curves represent configurations with InGaAs terminated by As and In, respectively. The right part of Figure 3 shows an energy-resolved contact resistance, defined by

$$R_c(E) = \frac{1}{T_{dev}(E)} - \frac{1}{T_{InGaAs}(E)} \quad (3)$$

While the Ti-InGaAs transmission for the two terminations are generally quite similar, close to the Fermi level the As-surface configuration gives a significantly larger transmission and hence a lower contact resistance. Similar looking curves are obtained for different metals and will not be presented here.

III. RESULTS

Figure 4 shows the specific contact resistivities vs. doping level for the Ti-InGaAs interfaces with either In or As surface termination as well as for a Ti-InAs interface. The stars show experimentally obtained values from Refs. [5], [10], [11], [12]. We observe that the agreement between calculated and experimental values is very satisfying. The lower contact resistance for the As surface is also observed for W-InGaAs interfaces, while we observe the opposite result for Mo-InGaAs contacts, c.f. Table I.

The decreasing contact resistance vs. doping is a general trend that we observe for all metals. The dashed line in Fig. 4 is

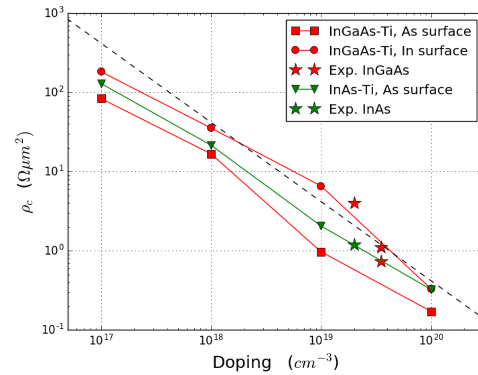

Fig. 4. Specific contact resistivity vs. doping for Ti-$In_{0.5}Ga_{0.5}As$ interfaces for In and As terminated surfaces (red curves) and for Ti-InAs intarfaces. The dashed black line is a trend line, with the form $\rho_c(n) = \alpha/n$, where n is measured in units of cm^{-3} and $\alpha = 2.74 \cdot 10^{11}\Omega\mu m^2$. The experimental data points are from Refs. [5], [10], [11], [12].

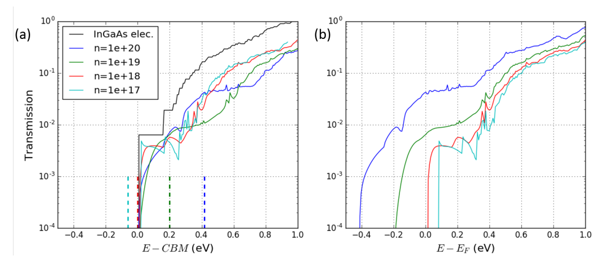

Fig. 5. Transmission spectra for the Ti-InGaAs interface (As terminated surface) vs. $E - E_F$ (a) and vs. $E - CMB$ (b), where CMB is the conduction band minimum. From panel (b), is is evident that the large change in doping doesn't affect the transmission spectrum significantly, but mainly shift the Fermi levels, indicated by vertical dashed lines.

a trend line with a $1/n$ dependence showing that the calculated contact resistivity is approximately inversely proportional to the doping concentration.

It is important to understand the origin of this doping dependence. In order to shed light on this we show in Fig. 5 the transmission spectra for Ti-InGaAs (As terminated surface) for the different dopings. In panel (a) we plot the transmissions vs. $E - CBM$, i.e. the conduction band minima (CBM) are aligned at 0 eV. Together with the transmissions through the Ti-InGaAs interface at different dopings (colored curves) we also show the transmission of a pure InGaAs device (black curve), which sets an upper bound of the device transmissions. The vertical dashed lines mark the Fermi levels at the different doping concentrations. From this plot we see that the transmission functions for the different doping levels is more or less the same. This shows that the main effect of increasing the doping level is to shift the Fermi level to energies where the transmission is high, and not to increase the transmission function it-self. In panel (b) we plot the transmissions vs. $E - E_F$, i.e. the Fermi levels are aligned at 0 eV. From this plot it is clear that increasing the doping level increases the transmission at the Fermi level (0 eV), which leads to a lower contact resistance.

In Fig. 2 we observed that the IV-curve is linear showing that the contact is Ohmic, and not dominated by tunneling through a Schottky barrier. The independence of the transmissions functions in Fig. 5 (b) also shows that the transport across the Ti-InGaAs interface is not dominated by tunneling. To further investigate the physics at the metal-InGaAs interface and the potential Schottky barrier formation, we show in Fig. 6 the local density of states (LDOS) vs. z-coordinate and energy for the As terminated surface at different doping levels. The black regions in the figures show the band gap in the InGaAs while the bright regions to the left in each plot show the high density of states in the Ti. Together with the LDOS plot we also plot the difference Hartree potential as obtained from the self-consistent DFT calculations [9]. The difference potential is aligned with the InGaAs CBM at the right electrode. While a clear potential barrier is formed at $n = 10^{19}$ cm^{-3} and $n = 10^{20}$ cm^{-3}, the top of the barrier is below the Fermi energy (0 eV in all plots, indicated by while dashed line), and the transport across the interface it therefore not dominated by tunneling, as confirmed by the linear IV-curve. For $n = 10^{19}$ cm^{-3} and $n = 10^{20}$ cm^{-3} we notice that the transmission close to the CBM, see Fig. 5, is indeed significantly suppressed due to the barrier formation. However, since this occurs way below the Fermi level, it is not important for the contact resistance. For $n = 10^{18}$ cm^{-3}, the potential is essentially flat, and we observe significantly larger transmission values close to the band edge, since there is no barrier to tunnel through.

The LDOS plots also show the formation of metal induced gap states (MIGS) that exist in InGaAs close to the interface at energies in the InGaAs band gap. These states decay exponentially away from the interface, but are clearly present in the InGaAs up to distance of ~ 5 nm from the interface.

IV. Conclusion

We have calculated specific contact resistivities of metal-$In_{0.5}Ga_{0.5}As$ and metal-InAs interfaces, where the metals studied are Ti, W, and Mo. In agreement with experiments, we find that the interfaces form Ohmic contacts at the experimentally relevant doping densities $n \sim 10^{19}$cm^{-3}. As a general trend we find that the contact resistance is approximately inversely proportional to the doping concentration. For both $In_{0.5}Ga_{0.5}As$ and InAs interfaces we find a close agreement between calculated and experimentally determined specific contact resistivities. The close agreement between DFT-calculated contact resistivities and experimental values is very promising. Future work will be devoted to studying more metals for which experimental results are not available in order to find promising candidate metals for low contact resistances.

Acknowledgment

The research leading to these results has received funding from the European Communitys Seventh Framework Programme (FP7/2007-2013) under grant agreement III-V-MOS Project n619326).

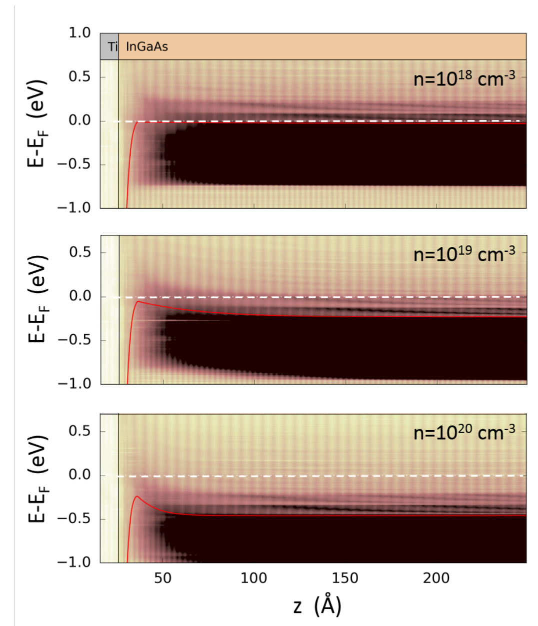

Fig. 6. Local density of states (LDOS) vs. z-coordinate and energy for the As terminated surface at different doping levels. The red curves in each plot show the Hartree difference potential obtained from the DFT calculations. The potential has been aligned with the CBM at the right electrode. The white dashed lines indicate the Fermi level.

References

[1] P. Krogstrup, N. L. B. Ziino, W. Chang, S. M. Albrecht, M. H. Madsen, E. Johnson, J. Nygaard, C. Marcus, and T. S. Jespersen, "Epitaxy of semiconductor-superconductor nanowires," *Nat Mater*, vol. 14, no. 4, pp. 400–406, Apr. 2015.

[2] "International technology roadmap for semiconductors: Emerging research materials,," Tech. Rep., Aug. 2013.

[3] R. Bjørk, "An analytical model for the influence of contact resistanceon thermoelectric efficiency," *Journal of Electronic Materials*, vol. 45, no. 3, pp. 1301–1308, 2016.

[4] "Atomistix toolkit version 2016, quantumwise a/s." [Online]. Available: www.quantumwise.com

[5] T. Markussen, K. Stokbro, M. Rau, M. Luisier, and A. Schenk, "D2.4: Physics-based simulations of leakage currents and contact resistance," 2016.

[6] "Advanced device relaxation tutorial." [Online]. Available: http://docs.quantumwise.com/tutorials/

[7] J. P. Perdew, K. Burke, and M. Ernzerhof, "Generalized Gradient Approximation Made Simple," *Phys. Rev. Lett.*, vol. 77, no. 18, pp. 3865–3868, 1996.

[8] F. Tran and P. Blaha, "Accurate Band Gaps of Semiconductors and Insulators with a Semilocal Exchange-Correlation Potential," *Phys. Rev. Lett.*, vol. 102, no. 22, p. 226401, jun 2009.

[9] D. Stradi, U. Martinez, A. Blom, M. Brandbyge, and K. Stokbro, "General atomistic approach for modeling metal-semiconductor interfaces using density functional theory and nonequilibrium green's function," *Phys. Rev. B*, vol. 93, p. 155302, Apr 2016.

[10] A. M. Crook, E. Lind, Z. Griffith, M. J. W. Rodwell, J. D. Zimmerman, A. C. Gossard, and S. R. Bank, "Low resistance, nonalloyed ohmic contacts to ingaas," *Applied Physics Letters*, vol. 91, no. 19, 2007.

[11] A. Baraskar, M. A. Wistey, V. Jain, E. Lobisser, U. Singisetti, G. Burek, Y. J. Lee, B. Thibeault, A. Gossard, and M. Rodwell, "Ex situ ohmic contacts to n-ingaas," *Journal of Vacuum Science & Technology B*, vol. 28, no. 4, pp. C5I7–C5I9, 2010.

[12] A. Baraskar, V. Jain, M. A. Wistey, U. Singisetti, Y.-J. Lee, B. Thibeault, A. Gossard, and M. J. W. Rodwell, "High doping effects on in-situ Ohmic contacts to n-InAs," in *Indium Phosphide Related Materials (IPRM), 2010 International Conference on*, 2010, pp. 1–4.